Journal of Orthopaedic Translation 51 (2025) 68–81

Contents lists available at ScienceDirect

Journal of Orthopaedic Translation

journal homepage: www.journals.elsevier.com/journal-of-orthopaedic-translation

Original Article

Fibroblast growth factor receptor 3 mutation promotes HSPB6-mediated cuproptosis in hypochondroplasia by impairing chondrocyte autophagy

Jing Chen [a], Dan He [a], Chengrun Yuan [a], Na Li [c], Baohong Shi [c], Conway Niu [d], Jiangfei Yang [e], Liangkai Zheng [f], Lin Che [b,**], Ren Xu [c,*]

[a] Department of Child Health, Department of Pediatrics, Women and Children's Hospital, School of Medicine, Xiamen University, Xiamen, Fujian, 361102, China
[b] State Key Laboratory of Oncology in South China, Guangdong Provincial Clinical Research Center for Cancer, Sun Yat-sen University Cancer Center, Guangzhou, Guangdong, 510060, China
[c] Fujian Provincial Key Laboratory of Organ and Tissue Regeneration, School of Medicine, Xiamen University, Xiamen, Fujian, 361102, China
[d] Department of General Paediatrics, Perth Children's Hospital, Nedlands, Western Australia, Australia
[e] Department of Radiology, Shandong Provincial Hospital Affiliated to Shandong First Medical University, Jinan, Shandong, 250021, China
[f] Department of Pathology, Women and Children's Hospital, School of Medicine, Xiamen University, Xiamen, Fujian, 361102, China

ARTICLE INFO

Keywords:
Autophagy
Cuproptosis
Fibroblast growth factor receptor 3
Heat shock protein B 6
mitochondrial fission
Hypochondroplasia

ABSTRACT

Background: Hypochondroplasia (HCH) is a prevalent form of dwarfism linked to mutations in the fibroblast growth factor receptor 3 (*FGFR3*) gene, causing missense alterations. We previous report was the first to identify *FGFR3*(G382D) gain-of-function variants with a positive family history as a novel cause of HCH. However, the precise contribution of *FGFR3* to the pathogenesis of HCH remains elusive.

Methods: We generated an *Fgfr3* (V376D) mutation mouse model using CRISPR/Cas9 technology and performed proteomic analyses to investigate the molecular mechanisms and potential therapeutic targets of HCH. Radiography and micro-computed tomography were employed to assess the bone-specific phenotype in *Fgfr3 (V376D)*mutant mice. Immunofluorescence, western blotting, and flow cytometry were used to systematically investigate the underlying mechanisms and therapeutic targets.

Results: We observed that *Fgfr3* (V376D) mutant mice exhibit a bone-specific phenotype, with symmetrically short limb bones, partially resembling the dwarfism phenotype of patients with HCH. We demonstrated that the mutant-activated FGFR3 promotes heat shock protein B 6 (HSPB6)-mediated cuproptosis by inhibiting chondrocyte autophagy both *in vivo* and *in vitro*. Additionally, we revealed that *FGFR3* (G382D) mutation leads to enhanced ERK signaling, increased Drp1-mediated mitochondrial fission, and upregulated cuproptosis-related protein ferredoxin 1 (FDX1). Furthermore, genetic and pharmacological inhibition of the HSPB6-ERK-Drp1-FDX1 pathway partially alleviate the phenotypes of *FGFR3* mutants.

Conclusions: Our study provides the first evidence for the pathogenicity of a gain-of-function mutation in *FGFR3* (G382D) using mouse and cell models, and it underscores the potential of targeting the HSPB6-ERK-Drp1-FDX1 axis as a novel therapeutic approach for HCH.

Translational potential of this article: We first demonstrate that impaired autophagy and enhanced cuproptosis are pivotal in the pathogenesis of HCH. This study not only enlarged the therapeutic potential of targeting cuproptosis for treating *FGFR3* mutation-related HCH but also provided a novel perspective on the role of the HSPB6-ERK-Drp1-FDX1 signaling pathway in the development of HCH. Consequently, this article provides valuable insights into the mechanisms and treatment strategies for *FGFR3* mutation-related chondrodysplasia.

* Corresponding author. State Key Laboratory of Cellular Stress Biology, Scholl of Medicine, Xiamen University, Yuejin Building. A503, Xiang'an South Road, Xiang'an District, Xiamen, 361102, China.
** Corresponding author.
E-mail addresses: chelin@sysucc.org.cn (L. Che), xuren526@xmu.edu.cn (R. Xu).

https://doi.org/10.1016/j.jot.2025.01.011
Received 4 June 2024; Received in revised form 15 December 2024; Accepted 20 January 2025

1. Introduction

Hypochondroplasia (HCH) is a skeletal dysplasia characterized by an autosomal-dominant inheritance pattern, resulting in excessive short stature and limb rhizomelia [1]. A precise diagnosis is essential because the clinical and radiological features of HCH are milder compared to other forms of dwarfisms, such as chondrodysplasia and thanatophoric dysplasia [2]. However, the pathogenic signaling pathways underlying HCH remains unclear, and its genetic aetiology remains to be elucidated.

Fibroblast growth factor receptor 3 (FGFR3) is a crucial receptor tyrosine kinase that regulates abnormal skeletal development [3,4]. Mutational activation of FGFR3 can lead to various congenital bone diseases, including HCH [5–7]. FGFR3 is known to play a significant role in skeletal development by interfering with chondrocyte proliferation through interactions with signaling pathways involved in chondrocyte formation [8,9]. This implies that constitutive activation of FGFR3 may impair bone formation. Interestingly, in *Fgfr3*$^{Y367C/+}$ mice, gain-of-function mutations in FGFR3 adversely affect bone growth via modulating defective ciliogenesis [10]. Moreover, it has been reported that impaired FGFR3 signaling affects downstream intracellular pathways, such as ERK1/2, contributing to the development of HCH [11]. Nonetheless, the precise molecular mechanism by which FGFR3 regulates chondrocyte proliferation and death is not yet fully understood. Therefore, it is imperative to elucidate the FGFR3 signaling pathway-dependent regulation of chondrocyte proliferation and death, as this could have significant implications for the diagnosis and treatment of HCH.

Autophagy is a lysosome-dependent catabolic process in which cytoplasmic components, including damaged or toxic proteins and organelles, are degraded to generate nutrient [12]. It has been identified as a critical regulatory mechanism for maintaining intracellular homeostasis and mediating pathological processes, including bone-related diseases [13]. Evidence suggests that dysregulation of lysosome-dependent autophagic pathways underlie skeletal pathologies resulting from impaired growth and differentiation of chondrocytes in the articular and growth plates [14,15]. Autophagy serves as a protective mechanism for chondrocytes under stress, such as hypoxia [14]. The inactivation of connective tissue growth factor CTGF/CCN2 in mice has been linked to chondrodysplasia due to its role in reducing autophagy and enhancing cell death [16]. On the other hand, gain-of-function mutations in FGFR3 have been found to inhibit autophagy in chondrocytes by decreasing the level of ATG12-ATG5 conjugate in *Fgfr3*$^{G369C/+}$ achondroplasia mice [17]. These findings suggest that abnormal cartilage development arises from the impairment of autophagy and the induction of cell death.

Yao et al. discovered that mitochondrial respiration is essential for cartilage development [18]. FGFR3-TACC3 activation stimulates mitochondrial respiration and biogenesis, leading to increased sensitivity to inhibitors of oxidative metabolism [19]. Studies have shown that ROS-mediated oxidative stress promotes catabolism by inducing cell death, which can disrupt cartilage homeostasis and is a major factor in chondrocyte damage [20,21]. As the primary source of ROS in cells, mitochondrial respiration dysfunction is proposed as a vital contributor to impaired cartilage development. Interestingly, Tsvetkov et al. demonstrated that cuproptosis, a recently discovered form of programmed cell death, is strongly associated with mitochondrial respiration and affects the tricarboxylic acid cycle [22]. Cuproptosis mediates a wide range of evolutionary processes in organisms, encompassing both health and disease, and is implicated in numerous physiological and pathological processes [23]. However, the molecular mechanisms linking autophagy to cartilage growth and the precise role of cuproptosis in HCH remain poorly understood.

In the present study, we investigated de novo mutations in the *FGFR3* gene identified in HCH patients based on our previous study [24]. Using both mouse and cell models, we explore the function and mechanisms of *FGFR3* (G382D) in HCH. Our findings provide evidence that inhibiting FGFR3 is necessary for maintaining articular cartilage, which is achieved by regulating the HSPB6-ERK-Drp1-FDX1 axis-mediated chondrocyte autophagy and cuproptosis. Our findings provide new insights into the pathophysiologic mechanisms and potential pharmacological targets for *FGFR3* mutation induces HCH.

2. Results

2.1. FGFR3 p.G382D in a patient with hypochondroplasia

We previously reported for the first time that *FGFR3* (G382D) gain-of-function variants with a family history were a novel cause of autosomal-dominant HCH with skeletal abnormalities [24]. To investigate the effects of *FGFR3* (G382D) mutation in individuals with skeletal anomalies, radiographic examinations were performed on a patient with HCH. The findings revealed that HCH patient exhibited irregular anterior edges of the lumbar vertebral bodies, depressed posterior edges of the vertebral bodies, reduced intervertebral distances from the lower thoracic to the lower lumbar vertebrae on both sides, a narrowed pelvis, and a widened and horizontal upper rim of the iliac acetabulum, compared to the normal control group (Fig. 1a and b). These observations suggest that *FGFR3* (G382D) gain-of-function mutations adversely affect skeletal growth and development.

2.2. Fgfr3 (V376D) mutation inhibits skeleton development in mice

To generate the mouse model of HCH and investigate the impact of *Fgfr3* gene mutation on development, we aimed to introduce the *Fgfr3* p.V376D mutation, corresponding to the human *FGFR3* p.G382D mutation, into the murine *Fgfr3* gene. The sgRNA sequence targeting exon 9 of murine *Fgfr3* gene (ENSMUST00000169212) with the c.[1127T > A] substitution for *Fgfr3* (V376D) was designed using the CRISPOR tool (Fig. 2a). Gene mutation analysis confirmed the successful generation of the *Fgfr3* (V376D) mouse model (Figs. S1a and S1b). To comprehensively evaluate the impact of the *Fgfr3* (V376D) mutation on skeletal development across different stages, we first investigated embryonic skeletal development. Employing Alcian blue and alizarin red S staining in E18.5 embryos, we observed that the *Fgfr3* (V376D) mutant mice exhibited significant delays in bone development, along with significant reductions in the lengths of the femur and tibia when compared to Wild-type (WT) (Fig. 2b). Next, WT and *Fgfr3* (V376D) littermates (heterozygote) were routinely fed for 10 weeks. Gross examination revealed that *Fgfr3* mutants exhibited varying degrees of reduced body length and limb shortening (Fig. 2c). Subsequently, X-ray images of the animals was obtained (Fig. 2d). The humeri and ulnas of the *Fgfr3* (V376D) mice were found to be shorter than those of the WT mice (Fig. 2e and f). Similarly, the femurs and tibias of the *Fgfr3* (V376D) mice exhibited decreased length compared to the WT mice (Fig. 2g and h).

Furthermore, high-resolution imaging of the mice revealed the bone-specific phenotype of HCH in the *Fgfr3* (V376D) mutants (Fig. 2i and j). The spine was shorter, the vertebral body volume and pelvis were smaller, and the acetabulum was shallower compared to those in the WT mice (Fig. 2i). The femur was thick and short, with a widened and deformed proximal metaphysis, and the femoral head epiphysis was not visible. The proximal tibia and fibula were shorter and smaller, the distal metaphysis was thickened, and the distal epiphysis was irregular (Fig. 2j). As shown in Fig. 2j, *Fgfr3* (V376D) mice had skeletal dysplasia with a reduced bone volume per tissue volume (BV/TV) in the femur, fibula, and tibia relative to the age-matched control littermates. Further analysis showed that the *Fgfr3* (V376D) mice displayed an increase in trabecular separation (Tb.Sp.) but a decrease in trabecular thickness (Tb.Th.) and trabecular number (Tb.N.). Additionally, to demonstrate whether there is a difference in chondrogenesis between WT and *Fgfr3* (V376D) mice, we extracted primary chondrocytes from postnatal day 5 WT and *Fgfr3* (V376D) mice. After 21 days of induced differentiation, we employed Alcian blue staining and observed a decrease in the cartilage

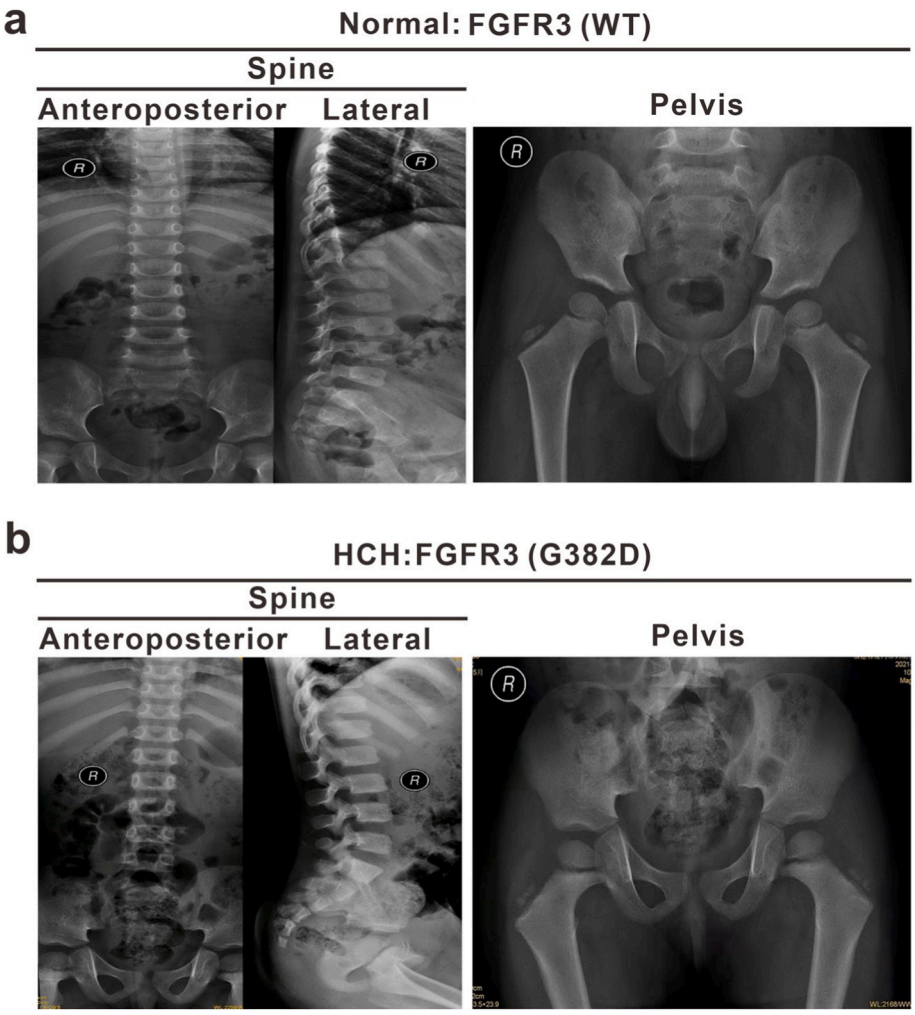

Fig. 1. Characteristics of HCH patient with *FGFR3* (G382D) mutations. **a** X-ray images of the spine and pelvis in the normal group. n = 1. **b** X-ray images of the spine and pelvis in a patient with HCH. n = 1.

matrix and diminished cartilage formation in the primary chondrocytes of *Fgfr3* (V376D) mice compared to those of WT mice (Fig. S1c). These results suggest that the *Fgfr3* (V376D) mutation inhibits chondrogenesis and skeletal development, resulting in the manifestation of a bone-specific phenotype of HCH in mice.

2.3. Proteomics coupled with bioinformatic analysis in mice with the *Fgfr3 (V376D)* mutation

Immunofluorescence staining results suggested that the FGFR3 protein expression level was significantly upregulated in the *Fgfr3* (V376D) mice compared to the WT mice, indicating that the mutation enhances FGFR3 expression (Fig. 3a). Besides, we extracted mesenchymal stem cells (MSCs) and osteoblasts (OBs) cells from WT and *Fgfr3* (V376D) mice, respectively. After osteogenic induction and differentiation, alizarin red staining revealed that compared to WT mice, the mineralized nodules in MSCs and OBs cells derived from *Fgfr3* (V367D) mice were significantly reduced (Fig. S2a). This suggests that the *Fgfr3* mutation impacts MSCs and OBs cells, leading to a decrease in the osteoblast differentiation and mineralization regulated by MSCs and OBs, which results in the reduced bone volume parameters in *Fgfr3* (V376D) mice. However, to identify proteins that are elevated or exclusive to the cartilage of mice with the *Fgfr3* (V376D) mutation versus WT mice, we performed label-free quantitative proteomics coupled with bioinformatic analysis on cartilage tissue samples from freshly frozen femur samples (n = 3 for WT mice and n = 3 mice for *Fgfr3* (V376D) mice, Fig. 3b). Applying a threshold of fold change ≥ 2 or ≤ -2, and $P < 0.05$, we identified 10 upregulated genes (indicated by red plots) and 13 downregulated genes (indicated by blue plots) in the *Fgfr3* (V376D) mice compared to the WT mice (Fig. 3c and Fig. S2b). Hierarchical clustering analysis comparing *Fgfr3* (V376D) mice and WT mice samples revealed that the levels of HSPB6 were significantly upregulated (fold change = 4.751) in the cartilage samples of *Fgfr3* (V376D) mice (Fig. 3d). The differentially expressed proteins were significantly enriched in organelles such as the nucleus, mitochondria, and lysosome (Fig. 3e).

To investigate the association between the *Fgfr3* (V376D) mutation and cell fate, we performed gene ontology (GO) enrichment analysis for biological processes (BP) to identify genes significantly impacted by the *Fgfr3* (V376D) mutation. We found that the "developmental process", "cell proliferation", and "growth" categories were significantly enriched in the cartilage tissue from *Fgfr3* (V376D) mice (Fig. 3f). The main molecular functions of the differential proteins were related to protein serine/threonine kinase activity (Fig. S2c). Kyoto Encyclopedia of Genes and Genomes (KEGG) enrichment analysis revealed that the differential proteins were significantly enriched in pathways related to "GnRH secretion", "Growth hormone synthesis and secretion pathway", "Gap junction", and other bone development-related pathways (Fig. S2d).

Furthermore, we verified the expression level of the HSPB6 protein through proteomic data analysis of the *Fgfr3* (V376D) site-directed mutation. The results demonstrated a significant upregulation of HSPB6 protein expression in the *Fgfr3* (V376D) mice compared to the WT mice (Fig. 3g). Immunofluorescence staining results suggested that

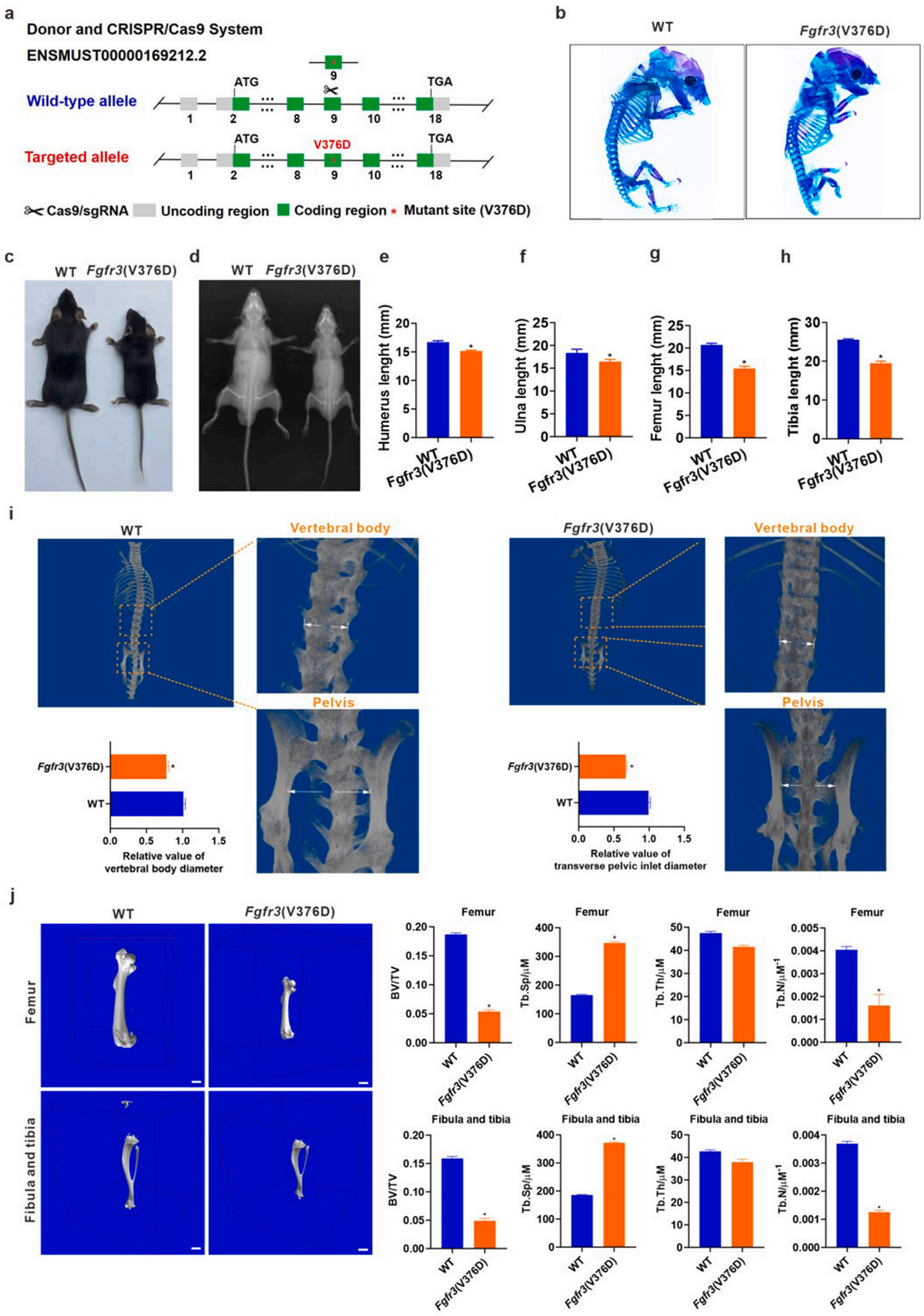

Fig. 2. *Fgfr3*(V376D) mutation inhibits skeleton development in mice. **a** Schematic diagram of the construction of *Fgfr3* (V376D) gene site-directed mutant mice by CRISPR/Cas9. **b** Skeletal preparations from E18.5 WT and *Fgfr3* (V376D) embryos were double-stained with alcian blue and alizarin red S. **c** General view of mice. **d-h** Radiographs of WT and *Fgfr3*(V376D) mice (heterozygote) and graphical representations of the humerus lengths (**e**), ulna lengths (**f**), femur lengths (**g**), and tibia lengths (**h**). **i** and **j** Bone-specific phenotypes observed by micro-CT imaging. Representative images of spine and pelvis (**i**), femur, fibula and tibia **(j)**. Quantitative parameters of micro-CT, including bone volume per tissue volume (BV/TV), trabecular space (Tb.Sp.), trabecular thickness (Tb.Th.), and trabecular number (Tb.N.). n = 3. $^{*}P < 0.05$ as compared to the WT mice.

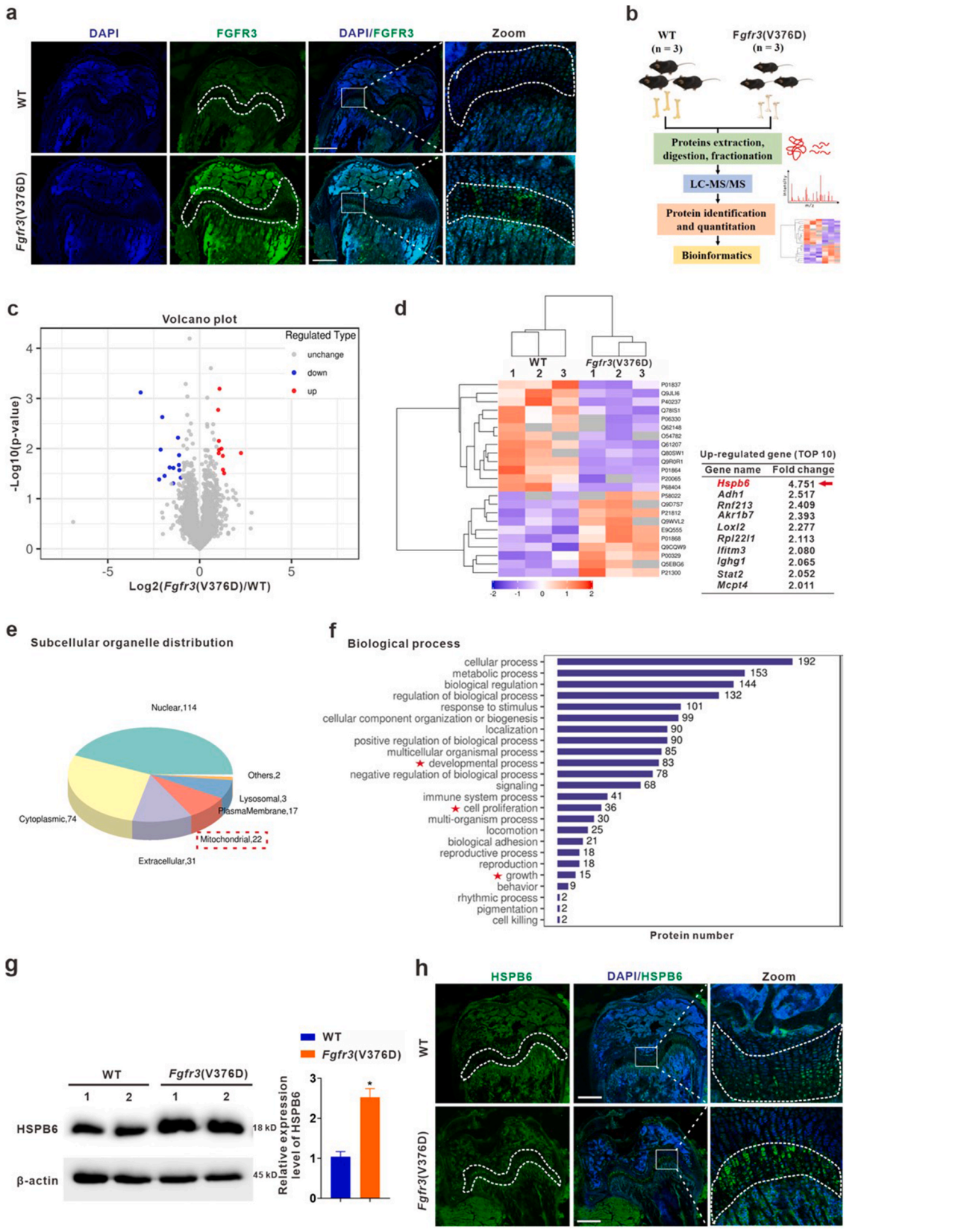

Fig. 3. Proteomics coupled with bioinformatic analysis of mice with *Fgfr3* (V376D) mutation. **a** Representative images for evaluating the expression of FGFR3. DAPI (Blue), nucleus. Scale bars, 250 μm **b** Schematic diagram of differentially expressed proteins (DEPs) in samples of *Fgfr3* (V376D) mice by proteomics combined with bioinformatics analysis. WT, n = 3; *Fgfr3* (V376D), n = 3. **c** Volcano plot was displayed for DEPs analysis. **d** The heatmap of DEPs in the *Fgfr3* (V376D) mice and the WT mice samples. **e** Distribution of subcellular organelle localization of DEPs. **f** GO enrichment was displayed for biological process analysis. **g** The protein levels of HSPB6 was detected by western blot. WT, n = 2; *Fgfr3* (V376D), n = 2. **h** Representative images for evaluating the expression of HSPB6 (green). DAPI (Blue), nucleus. Scale bars, 250 μm $^{*}P < 0.05$ as compared to the WT mice.

the HSPB6 level was significantly upregulated in the growth plate of *Fgfr3* (V376D) mice (Fig. 3h). These findings suggest that the regulation of chondrocyte growth and development-related signaling pathways by organelles, such as mitochondria, may be associated with FGFR3-HSPB6-mediated protein kinase signaling.

2.4. FGFR3 inhibits chondrocyte autophagy and proliferation, and promotes cuproptosis in Fgfr3 (V376D) mice

Autophagy is crucial for cell growth and development in chondrocytes. In this study, we aimed to investigate the involvement of autophagy in the pathogenesis of hereditary HCH. To explore the role of autophagy in skeletal dysplasia related to the *FGFR3* (G382D) mutation, we utilized *Fgfr3* (V376D)-mutated HCH mice. Firstly, the results of tissue immunofluorescence revealed that there was no significant change in the apoptosis marker protein Cleaved-Caspase-3 in *Fgfr3* (V376D) mice when compared to WT mice. However, the autophagy marker protein LC3B was significantly reduced (Figs. S3a and S3b). Subsequent isolation of primary chondrocytes and results indicate that, in comparison to the primary chondrocytes from WT mice, the level of LC3B decreased and the level of p62 increased in the primary chondrocytes of *Fgfr3* (V376D) mice, with no significant alteration in the apoptosis marker protein Cleaved-Caspase-3 (Fig. S3c). Moreover, the western blot analysis results from the cartilage tissue confirmed this observation, indicating that the mutation inhibits chondrocyte autophagy (Fig. 4a). To further investigate the impact of *Fgfr3* (V376D) mutation on cell proliferation, immunofluorescence staining results suggest that the Ki67 expression is downregulated in HCH mice with *Fgfr3* (V376D) mutation (Fig. 4b). Additional analysis revealed decreased levels of collagen 2A1 (COL2A1) and indian hedgehog (IHH) in the *Fgfr3* (V376D) mice (Fig. 4c and d). These results suggest that FGFR3 inhibits chondrocyte autophagy and proliferation. Furthermore, the results revealed a significant downregulation of the osteogenesis marker osteopontin (Spp1) in *Fgfr3*(V376D) mice compared to WT mice, suggesting that the *Fgfr3*(V376D) mutation may also lead to reduced osteogenesis (Fig. S3d).

Since mitochondria are key regulators in maintaining cartilage homeostasis, dynamic regulation of mitochondria may play an important role in cartilage growth and development [25]. Proteomic analysis comparing the *Fgfr3* (V376D) mice and the WT mice samples revealed that the levels of mitochondrial fission-related gene *Dnm1l*, tricarboxylic acid cycle-related gene pyruvate dehydrogenase kinase 1 (*Pdk1*), and copper-dependent lysyl oxidase-like 2 (*Loxl2*) were significantly upregulated in the *Fgfr3* (V376D) mice cartilage tissues (Fig. 4e), suggesting that *Fgfr3* (V376D) mutation may be involved in mitochondrial dynamics, the TCA process, and cuproptosis of chondrocytes. It was suggested that the expression level of the cuproptosis-related protein ferredoxin 1 (FDX1) was increased in the growth plate of *Fgfr3* (V376D) mice, and the activity of downstream molecules (phosphorylation of ERK) of FGFR3 and the mitochondrial fission protein Drp1 were also significantly upregulated (Fig. 4f and g). Furthermore, to investigate whether Drp1-mediated mitochondrial fission affects chondrocyte autophagy, we treated the primary chondrocytes of *Fgfr3* (V376D) mice with the Drp1 inhibitor Midvi-1. Compared to the control group, the expression of COL2 was enhanced, indicating that inhibiting mitochondrial fission can ameliorate the pathological phenotype of chondrocytes (Fig. S3e). This implies that chondrocyte autophagy is compromised in *Fgfr3* (V376D) mice, and inhibiting mitochondrial fission can promote chondrocyte proliferation. Histological examination of HCH femurs showed adipocyte expansion, reduced palisade cells in the proliferative zone, and primary lamellae in the osteoid zone (Fig. 4h). Collectively, these data suggest that FGFR3 inhibits autophagy and cell proliferation, and promotes cuproptosis in growth plate chondrocytes via the HSPB6-ERK-Drp1 signaling pathway (Fig. 4i).

2.5. FGFR3 negatively regulates cell autophagy and proliferation, and promotes cuproptosis in FGFR3 (G382D) chondrocytes

To investigate the impact of autophagy in HCH induced by FGFR3 mutation, we employed ATDC5 chondrocytes to expore the effect of FGFR3 on autophagy and cell proliferation. First, we constructed the pCDH-EF1-*FGFR3*-WT-Flag-T2A-Puro expression plasmid, and then the pCDH-EF1-*FGFR3*-G382D-Flag-T2A-Puro plasmid was constructed by site-directed mutagenesis, and *FGFR3* (G382D) of ATDC5 chondrocytes were established (Fig. 5a). Mutation analysis confirmed the successful construction of the ATDC5-*FGFR3* (G382D) cell model (Fig. 5b). Initially, we confirmed that the gain-of-function mutants of *FGFR3* (G382D) resulted in increased expression of FGFR3 and HSPB6 (Fig. 5c). Subsequently, we observed that the gain-of-function mutants of *FGFR3* (G382D) augmented the FGFR3-mediated increase in p-ERK, LC3A, and p62, while decreasing LC3B expression in ATDC5 cells (Fig. 5d and e). These findings that FGFR3 (G382D) mutants are activated through the HSPB6-ERK signalling pathway, leading to impaired autophagy in chondrocytes.

Additionally, the results found that *FGFR3* (G382D) cells showed an increase in FDX1 levels, while Ki67 levels decreased (Fig. 5f). The growth rate of both WT and *FGFR3* (G382D) cells was significantly decreased compared to the control cells, with *FGFR3* (G382D) cells showing a more pronounced inhibition of cell viability (Fig. 5g). Subsequent isolation of primary chondrocytes indicated that, compared to the primary chondrocytes from WT mice, the level of Ki67 was reduced in the primary chondrocytes of *Fgfr3* (V376D) mice (Fig. S4). Furthermore, flow cytometric analysis showed that *FGFR3* (G382D) cells had an increased number of cells in G2 cell cycle arrest compared to the WT and control cells (Fig. 5h). These data suggest that the gain-of-function mutants of *FGFR3* (G382D) inhibit proliferation and promotes HSPB6-ERK-mediated cuproptosis by impairing chondrocyte autophagy.

2.6. Rescue of FGFR3 (G382D)-induced cuproptosis by promoting chondrocyte autophagy

To investigate the impact of targeted autophagy inhibition on cartilage growth, we first used the CRISPR-Cas9 system to construct HSPB6 knockdown ATDC5 cells (Fig. 6a). Gene analysis confirmed the successful construction of the recombinant plasmid with HSPB6 knockdown (Figs. S5a–c). To further validate the impact of HSPB6 loss-of-function, we established stable HSPB6-knockdown ATDC5-Cas9-*HSPB6* (sgRNA1, sgRNA2, and sgRNA3) cell lines and confirmed their knockdown efficiency (Fig. 6b and c). Based on the efficiency of cell knockdown, we selected HSPB6-sgRNA2 cells for subsequent experiments.

Trametinib, an FDA-approved inhibitor of the MEK-ERK signaling pathway, is known for its ability to promote chondrocyte proliferation. To explore the biofunction function of targeting HSPB6 in conjunction with ERK pathway intervention, immunofluorescence assays revealed a decrease in LC3B protein expression and lysosome number, as well as a reduction in the co-localized distribution of LC3B and lysosome yellow fluorescent foci in the *FGFR3*(G382D) cells compared to the WT cells (Fig. 6d). Furthermore, targeting HSPB6 in combination with p-ERK intervention enhanced LC3B protein expression and lysosome number, and increased the co-localized distribution of LC3B and lysosome yellow fluorescent foci compared to the corresponding control cells (Fig. 6d). In HSPB6 knockdown cells, the *FGFR3* (G382D)-induced p-ERK and FDX1 expression was inhibited, while Ki67 expression was increased (Fig. 6e and f). Similarly, the Trametinib treatment group exhibited a significant decrease in p-ERK and FDX1 expression, with a concomitant increase in Ki67 expression, relative to the corresponding control cells (Fig. 6e and f). Furthermore, the autophagy activator rapamycin (Rapa) was used to induce chondrocytes autophagy, and it significantly reduced *FGFR3* (G382D)-induced FDX1 expression, suggesting that autophagy activation effectively alleviates cuproptosis in *FGFR3* (G382D) cells (Fig. S5d).

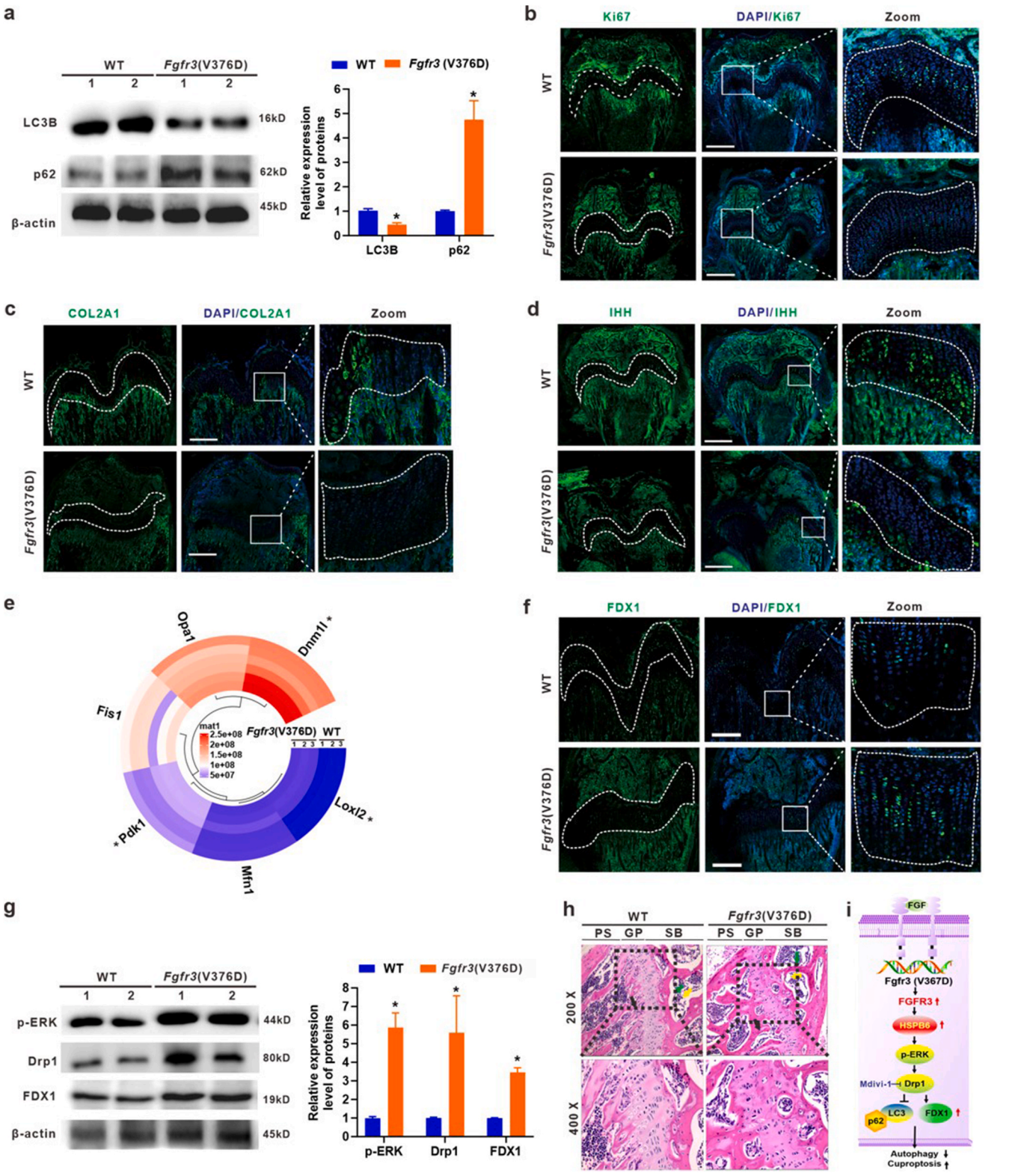

Fig. 4. FGFR3 inhibits chondrocyte autophagy and proliferation, promotes cuproptosis in *Fgfr3* (V376D) mice. **a** The protein levels of p62, and LC3B were detected by western blot. WT, n = 2; *Fgfr3* (V376D), n = 2. **b-d** Representative images for evaluating the expression of Ki67 (green), COL2A1 (green), and IHH (green). DAPI (Blue), nucleus. Scale bars, 250 μm. **e** The heatmap of differentially expressed proteins in the *Fgfr3* (V376D) mice and the WT mice samples. WT, n = 3; *Fgfr3* (V376D), n = 3. *$P < 0.05$ as compared to the WT group. **f** Representative images for evaluating the expression of FDX1 (green). DAPI (Blue), nucleus. Scale bars, 250 μm **g** The protein levels of p-ERK, Drp1 and FDX1 were detected by western blot. WT, n = 2; *Fgfr3* (V376D), n = 2. **h** Representative HE staining images were shown. **i** The schematic view of the FGFR3-HSPB6-p-ERK signaling pathway mediated autophagy inhibit and cuproptosis in growth plate chondrocytes. *$P < 0.05$ as compared to the WT mices.

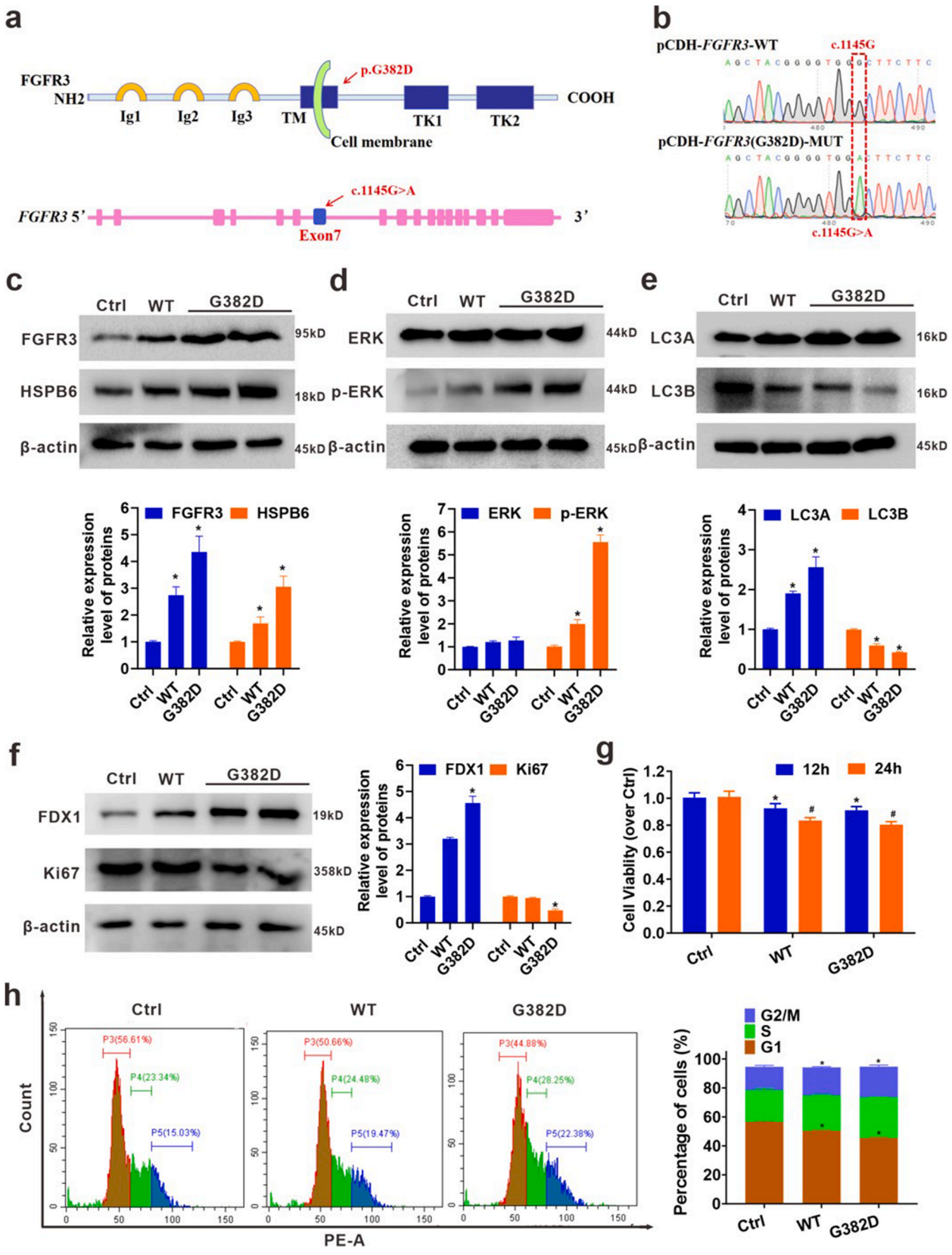

Fig. 5. FGFR3 negatively regulates cell autophagy and proliferation, promotes cuproptosis in *FGFR3* (G382D) chondrocytes. **a** An overview of human FGFR3 protein structure with indicated positions of the mutations (p.G382D). The positions of the mutations *FGFR3* (c.1145G > A) is located in 7 exons. **b** Sequencing maps of wild-type and mutant recombinant plasmids of *FGFR3* gene. **c-h** ADTC5-Ctrl, ADTC5-WT and ADTC5-*FGFR3* (G382) cells were used for the experiment. **c** The protein levels of FGFR3 and HSPB6 were detected by western blot. **d** The protein levels of ERK and p-ERK were detected by western blot. **e** The protein levels of LC3A and LC3B were detected by western blot. **f** The protein levels of FDX1 and Ki67 were detected by western blot. **g** Cell viability was detected by MTT assay. **h** Cell cycle were detected by flow cytometric. n = 3. $^{*}P < 0.05$ as compared to the ADTC5-Ctrl cells.

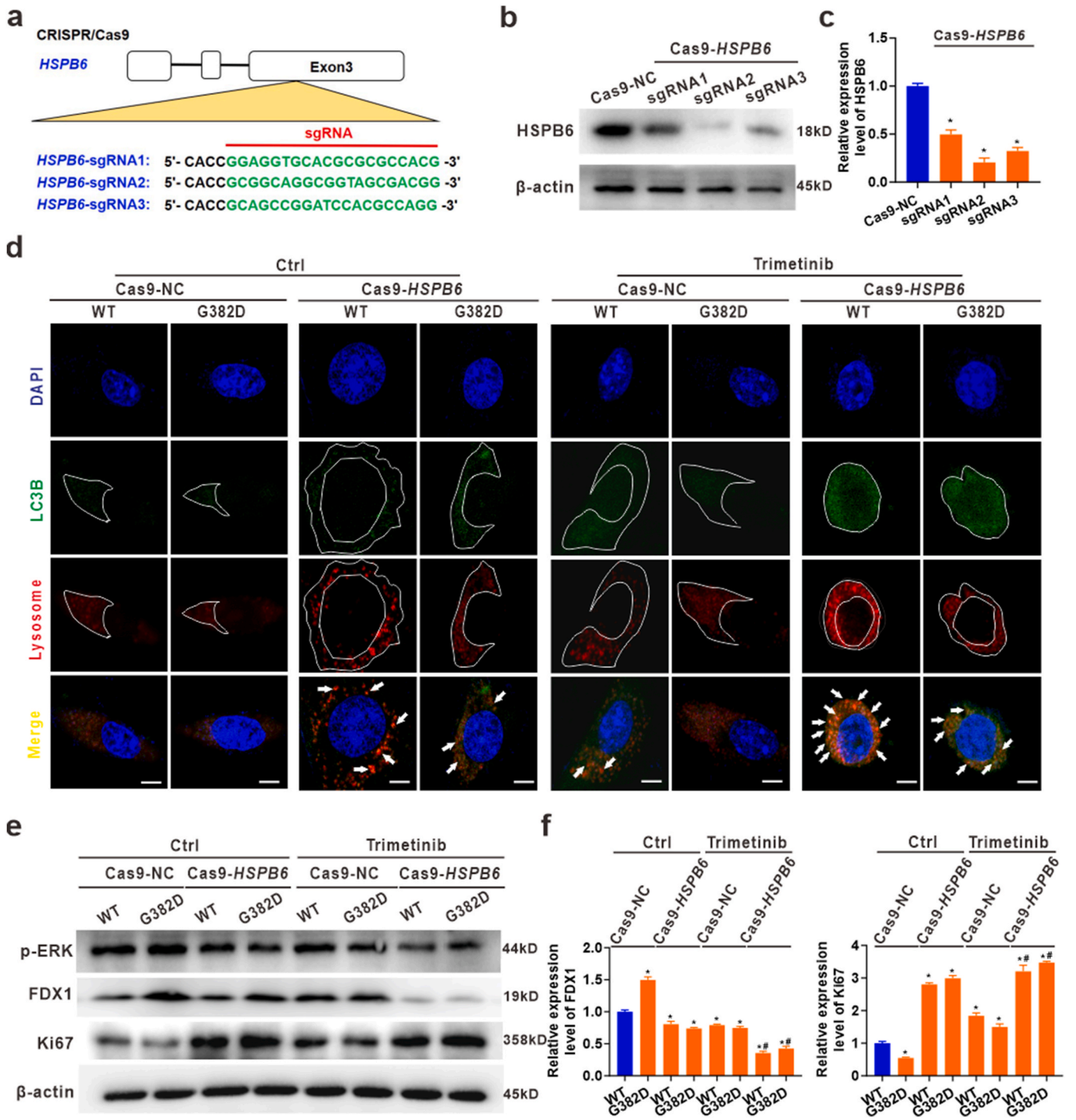

Fig. 6. Rescue of *FGFR3* (G382D)-induced cuproptosis by promoting chondrocyte autophagy. **a** Schematic diagram of the design of the HSPB6 knock down expression plasmid constructed by CRISPR-Cas9. **b, c** The protein levels of HSPB6 was detected by western blot. **d** Immunofluorescence representative images for evaluating the levels of LCB (green), Lysosome (red), and DAPI (blue) staining in cells. Scale bars, 10 μm. **e, f** The protein levels of p-ERK, FDX1 and Ki67 were detected by western blot. n = 3. $^{*}P < 0.05$ as compared to the ADTC5-WT cells. $^{\#}P < 0.05$ as compared to the ADTC5-*FGFR3* (G382D) cells.

These results indicate that the combined targeting of HSPB6 and ERK pathway intervention to activate autophagy rescues chondrocytes from *FGFR3* (G382D) mutation-induced cuproptosis.

2.7. Targeting HSPB6-Drp1-FDX1 axis intervention rescues FGFR3 (G382D)-induced chondrocyte cuproptosis

Cuproptosis has been shown to be closely associated with mitochondrial function [22]. To investigate the mitochondrial dynamic regulatory mechanism underlying chondrocyte death induced by the *FGFR3* (G382D) mutation, we assessed the mitochondrial function in chondrocytes. We found that the gain-of-function mutants of *FGFR3* (G382D) significantly enhanced the expression of the mitochondrial fission protein Drp1 (Fig. 7a). Immunofluorescence staining was used to observe the mitochondrial morphology (TOM20, a mitochondrial marker) in chondrocytes, revealing an elevated mitochondrial fission

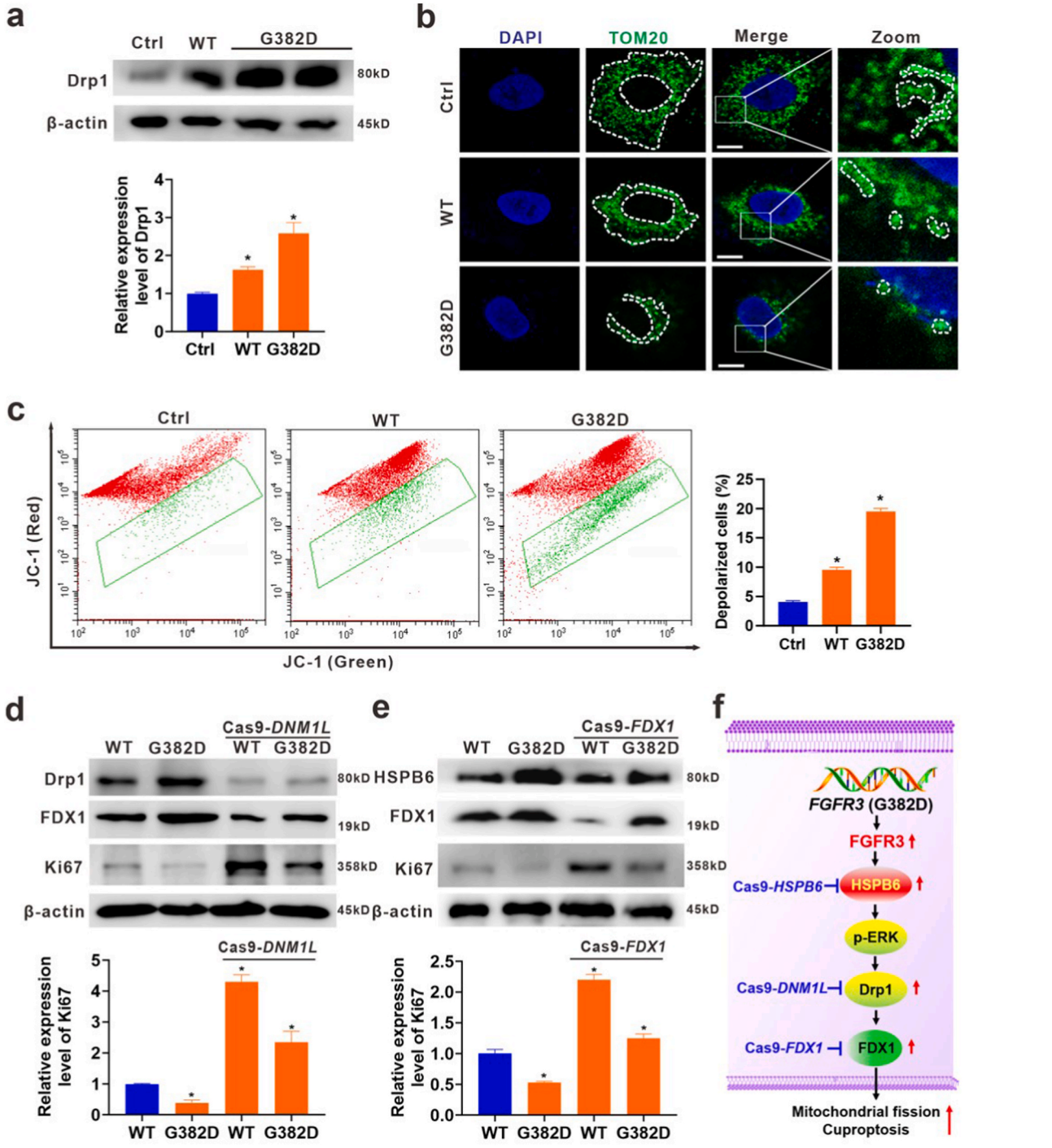

Fig. 7. Targeting HSPB6-Drp1-FDX1 axis intervention rescues *FGFR3* (G382D)-induced chondrocyte cuproptosis**. a-e** ADTC5-Ctrl, ADTC5-WT and ADTC5-*FGFR3* (G382) cells were used for the experiment. **a** The protein levels of Drp1 were detected by western blot. **b** Representative images show the mitochondrial morphology (TOM20, the outer membrane of mitochondria 20, green) captured by confocal microscopy. DAPI staining (blue), nucleus. Scale bars, 10 μm. **c** Cells were stained with JC-1 and detected by flow cytometry. Red and green fluorescence indicated JC-1 aggregates and JC-1 monomer, respectively. n = 3. $^*P < 0.05$ as compared to the ADTC5-Ctrl cells. **d** The protein levels of Drp1, FDX1, and Ki67 were detected by western blot. **e** The protein levels of HSPB6, FDX1, and Ki67 were detected by western blot. n = 3. $^*P < 0.05$ as compared to the ADTC5-WT cells. **f** The schematic view of the FGFR3-HSPB6-p-ERK-Drp1-FDX1 signaling pathway mediated mitochondrial fission and cuproptosis in chondrocytes.

rate in *FGFR3* (G382D) cells were increased compared to the control group (Fig. 7b). Our data also found that the mitochondrial membrane potential (Δψm) was decreased (with green fluorescence representing the JC-1 monomer indicative of low ΔΨm) in *FGFR3* (G382D) cells relative to the control group (Fig. 7c). These findings are in line with the *in vivo* experiments (Figs. 3e, 4e and 4g). Furthermore, targeting HSPB6 remarkably inhibited the expression of Drp1 and FDX1 in *FGFR3* (G382D) cells (Fig. S6a), indicating that Drp1-mediated excessive mitochondria fragmentation and decreased membrane potential may be involved in the onset of cuproptosis in *FGFR3* (G382D) cells.

To explore the effect of inhibiting Drp1-mediated mitochondria fission on cuproptosis in *FGFR3* (G382D) cells, we constructed Drp1 knockdown (Cas9-*DNM1L*) cells. The results showed a decreased in FDX1 protein expression and an increase in Ki67 expression (Fig. 7d),

suggesting that Drp1-mediated mitochondrial fission is involved in *FGFR3* (G382D)-induced chondrocyte cuproptosis. Subsequently, we constructed the FDX1 knockdown cells to detect the effect of targeted FDX1 on chondrocyte cuproptosis (Figs. S6b and S6c). The stable *FDX1* knockdown ATDC5-Cas9-*FDX1* (sgRNA1 and sgRNA2) cells were verified (Fig. S6d). The results showed no significant change in HSPB6 protein expression, but an increase in Ki67 expression compared to the corresponding control cells (Fig. 7e). These results indicate that targeting the HSPB6-Drp1-FDX1 axis rescues *FGFR3* (G382D)-induced mitochondrial fission and cuproptosis in chondrocyte (Fig. 7f).

3. Discussion

Bone development is a process strictly regulated by genes. Missense mutations in human FGFRs can lead to various congenital bone diseases, including chondrodysplasia syndromes [26]. Additionally, several integrated signaling pathways, such as Hedgehog (HH), parathyroid hormone-related protein (PTHrP), Wingless and int-1 (WNT), Transforming Growth Factor-β (TGF-β), and Bone Morphogenetic Protein (BMP), converge on specific transcription factors, including SRY-related HMG box 9 (SOX9), Runt-related transcription factor 2 (RUNX2), and Osterix (OSX) [27–29]. Dysregulation of these signaling pathways can result in a spectrum of bone diseases. The FGFR3 signaling pathway is an important regulator of skeletal development, and acquired mutations in the *FGFR3* gene lead to chondrodysplasia, such as HCH, through inhibiting chondrocyte proliferation by the activation of a kinase phosphorylation cascade signal [30,31]. AKT and ERK/p-ERK are involved in the pathogenesis of HCH caused by FGFR3 mutations [32,33]. In recent years, various therapeutic approaches with different molecular mechanisms have been developed using chondrodysplasia mouse models, including the use of C-type natriuretic peptide and tyrosine kinase activity inhibitors, among others [34,35]. While the efficacy and safety of these inhibitors require further investigation, a more detailed understanding of the molecular mechanisms will aid in developing improved diagnostic and therapeutic approaches for HCH.

Autophagy is essential in various physiological processes and the pathogenesis of several diseases [36]. It helps control the energy and internal environment of different cell types, including chondrocytes [37,38]. Maintaining an appropriate level of autophagy in the growth plate is essential for chondrocytes viability [39]. Dysfunctional autophagy, which leads to reduced chondrocyte viability, is thought to be one of the pathogenic mechanisms of chondrodysplasia [40]. HCH, a common genetic form of dwarfism in humans, is characterized by delayed skeletal growth and decreased cell viability, including reduced proliferation and increased apoptosis. In this study, we observed that hyperactivated FGFR3 promotes cuproptosis by impairing chondrocyte autophagy, as evidenced by the transformation of endogenous LC3 both *in vivo* and *in vitro*. Our findings reveal a novel link between FGFR3 signaling activation, autophagy, and cuproptosis in HCH. Impaired autophagy may represent a novel mechanism underlying FGFR3-related HCH pathogenesis.

Activation of a series of protein phosphorylation signaling pathways is involved in the execution of autophagy, with ERK/p-ERK being part of the core machinery [41–44]. In this study, proteomic analysis revealed a significant up-regulation of HSPB6 expression in the *Fgfr3* (V376D) mice compared to the WT mice. HSPB6, a heat shock protein, is primarily responsible for modulating cell survival in response to cellular stress. The present study implies that in the context of the *FGFR3* (G382D) mutation-associated cartilage disease model, the overexpression of HSPB6 may act as a pivotal intermediary, exacerbating disease progression through its impact on autophagy and cell proliferation in chondrocyte. In addition, the major functions of the differentially expressed proteins were related to protein kinase activity. Furthermore, we observed that gain-of-function mutants of *FGFR3* (G382D) augmented the FGFR3-mediated increase in p-ERK while decreasing Ki67 expression in chondrocytes. Our results suggest that FGFR3 inhibits autophagy and cell proliferation, and promotes cuproptosis in chondrocytes via the HSPB6-ERK-Drp1 signaling pathway. To investigate the impact of targeted inhibition of autophagy on cartilage growth, we explored the effect of targeted intervention of HSPB6 in combined with p-ERK intervention on chondrocyte growth. Our results indicate that autophagy activation rescues *FGFR3* (G382D) mutation-induced cuproptosis in chondrocyte. These findings suggest that manipulating the expression or activity of HSPB6 could be a promising strategy to rejuvenate autophagy in chondrocytes and to avert cuproptosis, thereby identifying potential therapeutic avenues for the management of *FGFR3* mutation-driven cartilage pathologies. Ultimately, the overexpression of HSPB6 in the context of FGFR3 mutation-associated suppression of chondrocyte autophagy and the potentiation of cuproptosis possesses profound biological implications. It may uncover previously uncharted signaling pathways and molecular interactions, thereby offering a fresh perspective on the complexities of chondrocyte biology. However, how HSPB6 is involved in FGFR3 mutation-induced impairment of chondrocyte autophagic activity through ERK/p-ERK signaling pathway activation requires further investigation.

Cuproptosis is a newly identified form of cell death that results from excessive copper and FDX1 accumulation in mitochondria [45]. Previous studies have demonstrated that FDX1 is the first protein found to regulate cuproptosis in eukaryotic cells [46,47]. These studies have provided comprehensive evidence suggesting the potential use of FDX1 as a therapeutic target for various diseases. However, the role of FDX1 in regulating mitochondrial dysfunction-mediated cuproptosis in skeletal development has been a subject of inquiry. In our study, we demonstrated that Drp1-mediated mitochondrial fission is involved in *FGFR3* (G382D)-induced chondrocyte cuproptosis. Further, targeting FDX1 intervention rescues *FGFR3* (G382D) mutation-induced chondrocyte cuproptosis. These results indicate that FDX1 is a key molecular player connecting mitochondrial dynamics and cartilage growth in HCH. Targeting the HSPB6-Drp1-FDX1 axis rescues *FGFR3* (G382D)-induced mitochondrial fission and cuproptosis in chondrocyte.

Our studies demonstrate that impaired autophagy and promoted cuproptosis play crucial role in the pathogenesis of HCH. We found that FGFR3 negatively regulates autophagy and promotes cuproptosis by activating the HSPB6-p-ERK-Drp1-FDX1 signaling pathway. Partially relieving of the inhibition of hyperactivated FGFR3 on chondrocyte viability and autophagy can be achieved by attenuating the activation of the HSPB6-p-ERK-Drp1-FDX1 signaling pathway (Fig. 8). These findings provide valuable insights into the mechanisms and potential treatment of FGFR3-related chondrodysplasia.

4. Materials and methods

4.1. Case studies

Consent from all participants or their legal guardians was acquired prior to their participation in this study. The Institutional Review Board (IRB) of Xiamen Maternal and Child Health Hospital (Xiamen, China) granted approval for the clinical investigations.

4.2. Mouse model generation

The CRISPOR Program was utilized to design the sgRNA sequence which targets exon 9 of murine *Fgfr3*(V376D). Brief, superovulated C57BL/6 mice were used to obtain one-cell stage embryos. These embryos were then injected with 10 ng μL of sgRNA and 20 ng single stranded repair template that introduces *FGFR3* (ENSMUST00000169212): c.[1127T > A] for the p.V376D substitution. Additionally, silent mutations were incorporated in the repair template to introduce a SalI restriction site and a degenerated PAM sequence. The Cas9 protein was jointly transfected with the repair template (5′-GGAGGAGCTGATGGAAACTGATGAGGCTGGCAGCGTGTACG-CAGGCGTCCTCAGCTATGGCGTCGACTTCTTCCTCTTCATCCTGGTGG

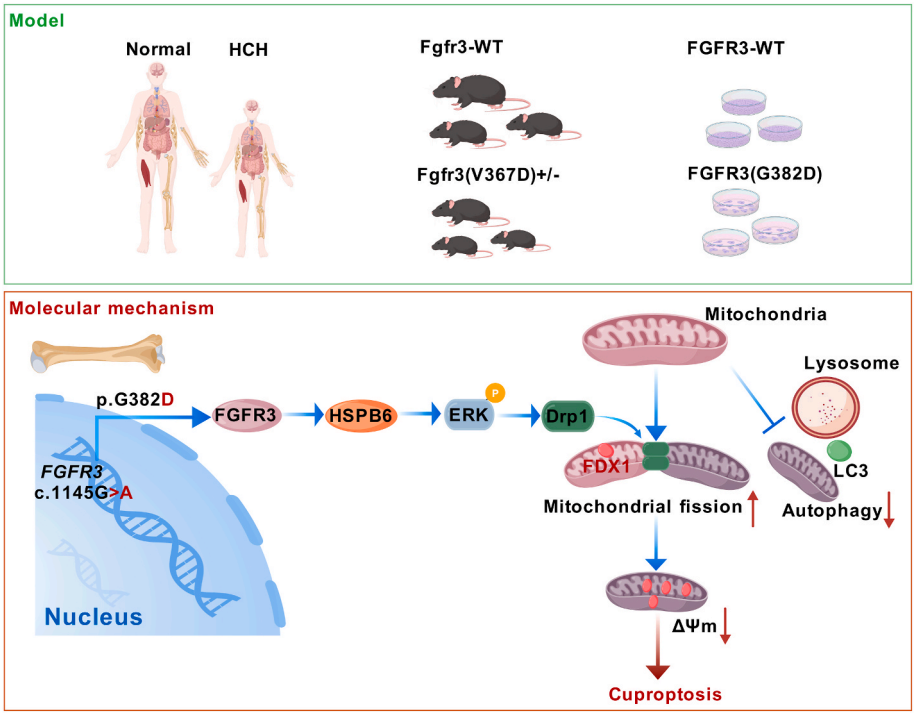

Fig. 8. *FGFR3* (G382D) mutation promotes HSPB6-mediated cuproptosis in hypochondroplasia by impairing chondrocyte autophagy. Our finding will provide new insights into the pathophysiologic mechanisms and the relevant pharmacological targets of FGFR3-related hypochondroplasia.

TGGCAGCTGTGATACTCTGCCGCCTGCGCAGTCCCCCAAAG) at a concentration of 50 ng μL. PCR was used to analyze the resulting offspring from embryos implanted into foster mothers. The PCR primers used were *Fgfr3*-F: 5′-TCTGCTGGGTTTCTCTCCTG-3′, *Fgfr3*-R: 5′-CTCTAGGAGACACGAGGCAG-3'. Additionally, SalI digestion was performed. To confirm the correct integration of the repair construct, sequence analysis was conducted. We successfully obtained an independent lineage with the *Fgfr3* c.[1127T > A] mutation (p.V376D). Both female and male mice were used in the experiment. All experimental procedures were carried out in accordance with the local animal care and protection guidelines.

4.3. Alcian blue and alizarin red S staining

Briefly, E18.5 embryos were fixed in 95 % ethanol for 24 h, stained in Alcian blue solution for 42 h, and then post-fixed in 95 % ethanol for 1 h per treatment, twice. Following this, they were treated with 2 % KOH for 3–4 h, stained with Alizarin red S solution for 3–4 h, and cleared in a 1 % KOH and 20 % glycerol solution.

4.4. Micro-computed tomography (CT) analysis

Femur, tibia and fibula samples were collected from WT, *Fgfr3* (V376D) mutant littermates of mice, as well as stripped of soft tissue and stored in 10 % formaldehyde in PBS for 48 h. The bones were scanned and analysis using micro-CT machine (SkyScan 1272 Bruker Belgium).

4.5. Preparation of primary chondrocytes

To obtain primary chondrocytes, cartilaginous tissue was carefully excised from the joint surface in a sterile environment, chopped into fine fragments, and subjected to triple rinsing with phosphate-buffered saline (PBS). The tissue pieces were then treated with 0.25 % Trypsin and kept at 37 °C for 30 min, followed by an incubation period in Dulbecco's Modified Eagle's Medium with high glucose (DMEM-HG; Invitrogen, Carlsbad, CA, USA) enriched with 2 % collagenase (Sigma–Aldrich, St. Louis, MO, USA) and 0.5 % dispase (Sigma–Aldrich) at 37 °C and 5 % CO2 for 4–6 h. Subsequently, the resulting cell suspension was filtered through a 40 μm filter to eliminate any debris, and the filtered cells were cultured in DMEM-HG supplemented with 10 % fetal bovine serum (FBS; Gibco, Grand Island, NY, USA) and 1 % antibiotic-antimycotic (Invitrogen) at 37 °C and 5 % CO2.

4.6. Proteomics analysis

Preparation of tissue protein samples and data analysis was performed by Applied Protein Technology (Shanghai, China).

4.7. Histology

The specific method was mentioned in our previous study [48]. Immunohistochemistry (IHC) staining was used to detect the levels of the indicated proteins (FGFR3, HSPB6, Ki67, IHH, COL2, and FDX1) through an IHC immunofluorescence assay. The slides were viewed using a laser-scanning confocal microscope (Leica SP8, Weztlar, CA, USA). Hematoxylin-eosin staining was performed on the specimen sections and counterstained with hematoxylin. All staining procedures were conducted according to the manufacturer's instructions.

4.8. Cell culture and treatments

Human embryonic kidney 293T (HEK293T) cells were preserved in our laboratory and cultured in Dulbecco's modified Eagle's medium (DMEM) supplemented with 10 % fetal bovine serum (FBS). ATDC5 cells were purchased from Xiamen Yimo Biotechnology and cultured in DMEM/F12 (1:1) supplemented with 5 % FBS. To initiate treatment, ATDC5 cells were exposed to trimetinib (50 nM) or rapamycin (Rapa, 20 μM) for a duration of 24 h.

4.9. Site-directed mutagenesis of FGFR3 (G382D)

Site-directed mutagenesis of *FGFR3* (G382D) was performed as

described in the previous method [48]. To generate a base mutation from glycine to aspartate (G to D) at position 382 of FGFR3, the pCDH-EF1-FGFR3-WT-Flag-T2A-Puro DNA template was amplified using two primers in the opposite direction. The resulting PCR products were self-ligated using T4 polynucleotide kinase. ATDC5 cells were then transfected with pCDH-EF1-FGFR3-G382D-flag-T2A-Puro at a concentration of 2 μg/mL using Lipofectamine® 2000 (Invitrogen).

4.10. Establishment of knockdown cell lines

The specific method was mentioned in the previous method [49]. The *HSPB6*-sgRNAs were annealed and cloned into the LentiCRISPRv2 vector (Watertown, MA, USA). The primer sequences were as followings: *HSPB6*-sgRNA1, forward primer (FP): 5′- CACCGGAGGTGCACGCGCGC-CACG -3′, reverse primer (RP): 5′-AAACCGTGGCGCGCGTGCACCTCC-3′. *HSPB6*-sgRNA2, FP: 5′-CACCGCGGCAGGCGGTAGCGACGG-3′ and RP: 5′-AAACCGTGGCGCGCGTGCACCTCC-3′. *HSPB6*-sgRNA3, FP: 5′-CACCG CAGCCGGATCCACGCCAGG-3′ and RP: 5′-AAACCCTGGCGTGGATCCG GCTGC-3′. Lenti-Cas9-*HSPB6*-expressing constructs or negative control (NC) plasmids were transfected into HEK293T cells. They were ATDC5-Cas9-*HSPB6* cells and their corresponding controls were ATDC5-Cas9-NC cells. As mentioned above, for the construction of Lenti-Cas9- *FDX1* plasmids, the primer sequences were as followings: *FDX1*-sgRNA1, FP: 5′-CACCGTCCACTTTATAAACCGTGA-3′ and RP: 5′-AAACTCACGGTTTATAAAGTGGAC-3′. *FDX1*-sgRNA2, FP: 5′-CACCGT GGCTTGTTCAACCTGTCAC-3′ and RP: 5′-AAACGTGACAGGTTGAACAA GCCAC-3′. They were ATDC5-Cas9-*FDX1* cells for *FDX1*-knockdown, and their controls were ATDC5-Cas9-NC cells.

4.11. Western blotting

Western blotting analysis was performed as previously described [50]. The protein bands of interest were incubated overnight at 4 °C with primary antibodies targeting specific proteins. Subsequently, the bands were incubated with the appropriate secondary antibodies. Western blot bands were visualized with an enhanced chemiluminescence kit, and the relative blot intensities were quantified using the Image J software (MD, USA). The primary antibodies were shown in Supplemental Table S1.

4.12. Immunofluorescence staining (IF) and confocal microscopy

IF assay was performed as previously described [50]. Briefly, at the end of the experiment, cells were fixed with 4 % paraformaldehyde for 1 h and permeabilized with methanol. Slides were then incubated with a blocking solution (1 % BSA) for 1 h, followed by exposure to anti-HSPB6, anti-p-ERK, anti-LCII, and anti-Ki67 antibodies at 4 °C overnight. After incubation with the primary antibody, slides were further incubated with secondary antibodies. The cells, counterstained with DAPI, were observed and recorded using a confocal microscope (Leica SP8, Weztlar, CA, USA). The primary antibodies were shown in Supplemental Table S2.

CRediT authorship contribution statement

Jing Chen: Conceptualization, Supervision, Investigation, Writing – original draft. **Dan He:** Investigation, Data curation. **Chengrun Yuan:** Data curation, Formal analysis. **Na Li:** Data curation. **Baohong Shi:** Data curation. **Conway Niu:** Writing – review & editing. **Jiangfei Yang:** Data curation. **Liangkai Zheng:** Data curation. **Lin Che:** Investigation, Data curation, Formal analysis, Writing – review & editing. **Ren Xu:** Conceptualization, Writing – review & editing, All authors discussed the results and commented on the manuscript.

5. Statistical analysis

Statistical analyses were conducted using the Statistical Package for Social Sciences (SPSS) version 20.0 (IBM Corp, Armonk, NY, USA). The data presented in this study were obtained from at least three independent experiments and are expressed as means ± standard deviation (SD). The Student's *t* test was used to evaluate the numeric data. A *p*-value of less than 0.05 was considered statistically significant.

Ethics statement

The animal study was reviewed and approved by Ethics Committee of the Xiamen University.

Declaration of competing interest

The authors declare that they have no competing interests.

Acknowledgements

This work was supported by the National Natural Science Foundation of China (Nos. 82103859 and 82304180), Fujian Province Natural Science Foundation (No. 2023J011602), Guangdong Basic and Applied Basic Research Foundation (No. 2024A1515010893), China Postdoctoral Science Foundation (No. 2022M713585).

Abbreviations

DMEM	dulbecco's modified Eagle's medium
FBS	fetal bovine serum
FDX1	ferredoxin 1
FGFR3	fibroblast growth factor receptor 3
FP	forward primer
GO	gene ontology
HCH	Hypochondroplasia
HSPB6	heat shock protein B
KEGG	kyoto encyclopedia of genes and genomes
Loxl2	lysyl oxidase-like 2
Pdk1	pyruvate dehydrogenase kinase 1
Rapa	rapamycin
RP	reverse primer
SD	standard deviation
WT	Wild-type

Appendix A. Supplementary data

Supplementary data to this article can be found online at https://doi.org/10.1016/j.jot.2025.01.011

References

[1] Bellus GA, McIntosh I, Smith EA, Aylsworth AS, Kaitila I, Horton WA, et al. A recurrent mutation in the tyrosine kinase domain of fibroblast growth factor receptor 3 causes hypochondroplasia. Nat Genet 1995;10:357–9.
[2] Kunova Bosakova M, Varecha M, Hampl M, Duran I, Nita A, Buchtova M, et al. Regulation of ciliary function by fibroblast growth factor signaling identifies FGFR3-related disorders achondroplasia and thanatophoric dysplasia as ciliopathies. Hum Mol Genet 2018;27:1093–105.
[3] Deng C, Wynshaw-Boris A, Zhou F, Kuo A, Leder P. Fibroblast growth factor receptor 3 is a negative regulator of bone growth. Cell 1996;84:911–21.
[4] Su N, Jin M, Chen L. Role of FGF/FGFR signaling in skeletal development and homeostasis: learning from mouse models. Bone Res 2014;2:14003.
[5] Foldynova-Trantirkova S, Wilcox WR, Krejci P. Sixteen years and counting: the current understanding of fibroblast growth factor receptor 3 (FGFR3) signaling in skeletal dysplasias. Hum Mutat 2012;33:29–41.
[6] Alatzoglou KS, Hindmarsh PC, Brain C, Torpiano J, Dattani MT. Acanthosis nigricans and insulin sensitivity in patients with achondroplasia and hypochodroplasia due to FGFR3 mutations. J Clin Endocrinol Metab 2009;94:3959–63.

[7] Yao G, Wang G, Wang D, Su G. Identification of a novel mutation of FGFR3 gene in a large Chinese pedigree with hypochondroplasia by next-generation sequencing: a case report and brief literature review. Medicine (Baltim) 2019;98:e14157.
[8] Kimura T, Bosakova M, Nonaka Y, Hruba E, Yasuda K, Futakawa S, et al. An RNA aptamer restores defective bone growth in FGFR3-related skeletal dysplasia in mice. Sci Transl Med 2021;13:eaba4226.
[9] Minina E, Kreschel C, Naski MC, Ornitz DM, Vortkamp A. Interaction of FGF, Ihh/Pthlh, and BMP signaling integrates chondrocyte proliferation and hypertrophic differentiation. Dev Cell 2002;3:439–49.
[10] Martin L, Kaci N, Benoist-Lasselin C, Mondoloni M, Decaudaveine S, Estibals V, et al. Theobroma cacao improves bone growth by modulating defective ciliogenesis in a mouse model of achondroplasia. Bone Res 2022;10:8.
[11] Olney RC, Prickett TC, Espiner EA, Mackenzie WG, Duker AL, Ditro C, et al. C-type natriuretic peptide plasma levels are elevated in subjects with achondroplasia, hypochondroplasia, and thanatophoric dysplasia. J Clin Endocrinol Metab 2015;100:E355–9.
[12] Kitada M, Koya D. Autophagy in metabolic disease and ageing. Nat Rev Endocrinol 2021;17:647–61.
[13] Pierrefite-Carle V, Santucci-Darmanin S, Breuil V, Camuzard O, Carle GF. Autophagy in bone: self-eating to stay in balance. Ageing Res Rev 2015;24:206–17.
[14] Madhu V, Guntur AR, Risbud MV. Role of autophagy in intervertebral disc and cartilage function: implications in health and disease. Matrix Biol 2021;100-101:207–20.
[15] Yan W, Zheng L, Xu X, Hao Z, Zhang Y, Lu J, et al. Heterozygous LRP1 deficiency causes developmental dysplasia of the hip by impairing triradiate chondrocytes differentiation due to inhibition of autophagy. Proc Natl Acad Sci U S A 2022;119:e2203557119.
[16] Hall-Glenn F, Aivazi A, Akopyan L, Ong JR, Baxter RR, et al. CCN2/CTGF is required for matrix organization and to protect growth plate chondrocytes from cellular stress. J Cell Commun Signal 2013;7:219–30.
[17] Wang X, Qi H, Wang Q, Zhu Y, Wang X, Jin M, et al. FGFR3/fibroblast growth factor receptor 3 inhibits autophagy through decreasing the ATG12-ATG5 conjugate, leading to the delay of cartilage development in achondroplasia. Autophagy 2015;11:1998–2013.
[18] Yao Q, Khan MP, Merceron C, LaGory EL, Tata Z, Mangiavini L, et al. Suppressing mitochondrial respiration is critical for hypoxia tolerance in the fetal growth plate. Dev Cell 2019;49:748–63. e747.
[19] Frattini V, Pagnotta SM, Tala, Fan JJ, Russo MV, Lee SB, et al. A metabolic function of FGFR3-TACC3 gene fusions in cancer. Nature 2018;553:222–7.
[20] Bolduc JA, Collins JA, Loeser RF. Reactive oxygen species, aging and articular cartilage homeostasis. Free Radic Biol Med 2019;132:73–82.
[21] Zhang Y, Hou M, Liu Y, Liu T, Chen X, Shi Q, et al. Recharge of chondrocyte mitochondria by sustained release of melatonin protects cartilage matrix homeostasis in osteoarthritis. J Pineal Res 2022;73:e12815.
[22] Tsvetkov P, Coy S, Petrova B, Dreishpoon M, Verma A, Abdusamad M, et al. Copper induces cell death by targeting lipoylated TCA cycle proteins. Science 2022;375:1254–61.
[23] Yang Y, Wu J, Wang L, Ji G, Dang Y. Copper homeostasis and cuproptosis in health and disease. MedComm 2020;5:e724. 2024.
[24] Chen J, Yang J, Zhao S, Ying H, Li G, Xu C. Identification of a novel mutation in the FGFR3 gene in a Chinese family with Hypochondroplasia. Gene 2018;641:355–60.
[25] Du X, Duan M, Kan S, Yang Y, Xu S, Wei J, et al. TGF-β3 mediates mitochondrial dynamics through the p-Smad3/AMPK pathway. Cell Prolif 2024;57:e13579.
[26] Su N, Jin M, Chen L. Role of FGF/FGFR signaling in skeletal development and homeostasis: learning from mouse models. Bone Res 2014;2:14003.
[27] Yi Dan, Xie Rong, Zeng Daofu, Xiao Jun, Xiao Guozhi, Jin Hongting, et al. Loss of Axin1 in limb mesenchymal cells leads to multiple synostoses syndrome-like phenotype in mice. Innovat Med 2024;2:100053.
[28] Xie R, Yi D, Zeng D, Jie Q, Kang Q, Zhang Z, et al. Specific deletion of Axin1 leads to activation of β-catenin/BMP signaling resulting in fibular hemimelia phenotype in mice. Elife 2022;11:e80013.
[29] Guasto A, Cormier-Daire V. Signaling pathways in bone development and their related skeletal dysplasia. Int J Mol Sci 2021;22:4321.
[30] Krejci P. The paradox of FGFR3 signaling in skeletal dysplasia: why chondrocytes growth arrest while other cells over proliferate. Mutat Res Rev Mutat Res 2014;759:40–8.
[31] Takemoto G, Matsushita M, Okamoto T, Ito T, Matsuura Y, Takashima C, et al. Meclozine attenuates the MARK pathway in mammalian chondrocytes and ameliorates FGF2-induced bone hyperossification in larval zebrafish. Front Cell Dev Biol 2021;9:694018.
[32] Ornitz DM, Marie PJ. Fibroblast growth factor signaling in skeletal development and disease. Genes Dev 2015;29:1463–86.
[33] Moon AM, Guris DL, Seo JH, Li L, Hammond J, Talbot A, et al. Crkl deficiency disrupts Fgf8 signaling in a mouse model of 22q11 deletion syndromes. Dev Cell 2006;10:71–80.
[34] Savarirayan R, Irving M, Bacino CA, Bostwick B, Charrow J, Cormier-Daire V, et al. C-Type natriuretic peptide analogue therapy in children with achondroplasia. N Engl J Med 2019;381:25–35.
[35] Savarirayan R, De Bergua JM, Arundel P, McDevitt H, Cormier-Daire V, Saraff V, et al. Infigratinib in children with achondroplasia: the PROPEL and PROPEL 2 studies. Ther Adv Musculoskelet Dis 2022;14. 1759720X221084848.
[36] Mizushima N, Levine B. Autophagy in human diseases. N Engl J Med 2020;383:1564–76.
[37] Cinque L, Forrester A, Bartolomeo R, Svelto M, Venditti R, Montefusco S, et al. FGF signalling regulates bone growth through autophagy. Nature 2015;528:272–5.
[38] Starling S. A role for autophagy in bone biology. Nat Rev Endocrinol 2019;15:438–9.
[39] Yang C, Xu X, Dong X, Yang B, Dong W, Luo Y, et al. DDIT3/CHOP promotes autophagy in chondrocytes via SIRT1-AKT pathway. Biochim Biophys Acta Mol Cell Res 2021;1868:119074.
[40] Vesela B, Svandova E, Ramesova A, Kratochvilova A, Tucker AS, Matalova E. Caspase inhibition affects the expression of autophagy-related molecules in chondrocytes. Cartilage 2021;13:956S–68S.
[41] Mahli A, Saugspier M, Koch A, Sommer J, Dietrich P, Lee S, et al. ERK activation and autophagy impairment are central mediators of irinotecan-induced steatohepatitis. Gut 2018;67:746–56.
[42] Zhang P, Holowatyj AN, Roy T, Pronovost SM, Marchetti M, Liu H, et al. An SH3PX1-dependent endocytosis-autophagy network restrains intestinal stem cell proliferation by counteracting EGFR-ERK signaling. Dev Cell 2019;49:574–89. e575.
[43] Stalnecker CA, Grover KR, Edwards AC, Coleman MF, Yang R, DeLiberty JM, et al. Concurrent inhibition of IGF1R and ERK increases pancreatic cancer sensitivity to autophagy inhibitors. Cancer Res 2022;82:586–98.
[44] Li M, Zhao X, Yong H, Shang B, Lou W, Wang Y, et al. FBXO22 promotes growth and metastasis and inhibits autophagy in epithelial ovarian cancers via the MAPK/ERK pathway. Front Pharmacol 2021;12:778698.
[45] Tang D, Chen X, Kroemer G. Cuproptosis: a copper-triggered modality of mitochondrial cell death. Cell Res 2022;32:417–8.
[46] Wang T, Liu Y, Li Q, Luo Y, Liu D, Li B. Cuproptosis-related gene FDX1 expression correlates with the prognosis and tumor immune microenvironment in clear cell renal cell carcinoma. Front Immunol 2022;13:999823.
[47] Zhang C, Zeng Y, Guo X, Shen H, Zhang J, Wang K, et al. Pan-cancer analyses confirmed the cuproptosis-related gene FDX1 as an immunotherapy predictor and prognostic biomarker. Front Genet 2022;13:923737.
[48] Che L, Du ZB, Wang WH, Wu JS, Han T, Chen YY, et al. Intracellular antibody targeting HBx suppresses invasion and metastasis in hepatitis B virus-related hepatocarcinogenesis via protein phosphatase 2A-B56gamma-mediated dephosphorylation of protein kinase B. Cell Prolif 2022;55:e13304.
[49] Che L, Wu JS, Du ZB, He YQ, Yang L, Lin JX, et al. Targeting mitochondrial COX-2 enhances chemosensitivity via Drp1-dependent remodeling of mitochondrial dynamics in hepatocellular carcinoma. Cancers 2022;14:821.
[50] Che L, Wu JS, Xu CY, Cai YX, Lin JX, Du ZB, et al. Protein phosphatase 2A-B56gamma-Drp1-Rab7 signaling axis regulates mitochondria-lysosome crosstalk to sensitize the anti-cancer therapy of hepatocellular carcinoma. Biochem Pharmacol 2022;202:115132.